6. Booth, J. S., Winters, W. J. & Dillon, W. P. Circumstantial evidence of gas hydrate and slope failure associations on US Atlantic continental margin. *Ann. N.Y. Acad. Sci.* **75,** 487–489 (1994).
7. Collett, T. S. & Kuuskraa, V. A. Hydrates contain vast store of world gas resources. *Oil Gas J.* 11 May, 90–95 (1998).
8. Gettrust, J. F., Ross, J. H. & Rowe, M. M. Development of a low frequency, deep-tow geoacoustics system. *Sea Technol.* **32,** 23–32 (1991).
9. Wood, W. T. & Gettrust, J. F. in *Natural Gas Hydrates: Occurrence, Distribution, and Dynamics* (eds Paull, C. K. & Dillon, W. P.) 165–178 (AGU Monograph no. 124, American Geophysical Union, Washington DC, 2001).
10. Westbrook, G. K., Carson, B., Musgrave, R. J. & Suess, E. *Proc. ODP Init. Rep.* **146** (1994).
11. Hyndman, R. D. & Spence, G. D. A seismic study of methane hydrate marine bottom-simulating reflectors. *J. Geophys. Res.* **97,** 6683–6698 (1992).
12. Chapman, N. R. *et al.* High-resolution, deep-towed, multichannel seismic survey of deep-sea gas hydrates off western Canada. *Geophysics* **67,** 1038–1047 (2002).
13. Xu, W. & Ruppel, C. Predicting the occurrence, distribution, and evolution of methane gas hydrate in porous marine sediments. *J. Geophys. Res.* **104,** 5081–5095 (1999).
14. Heggland, R., Meldahl, P., de Groot, P. & Aminzadeh, F. Chimney cube unravels subsurface. *Am. Oil Gas Reporter* 78–83 (February 2000).
15. Meldahl, P., Heggland, R., Bril, B. & de Groot, P. Identifying faults and gas chimneys using multiattributes and neural networks. *Leading Edge* **20,** 474–482 (2001).
16. Hovland, M. & Judd, G. *Seabed Pockmarks and Seepages* 181 (Graham & Trotman, London, 1988).
17. Voss, C. I. A finite element simulation model for saturated and unsaturated, fluid-density-dependent ground-water flow with energy transport or chemically reactive single species solute transport (USGS Water Resources Investigations Report 84–4369, 1984).
18. Brown, K. M., Bangs, N. L., Froelich, P. N. & Kvenvolden, K. A. The nature, distribution and origin of gas hydrate in the Chile Triple Junction region. *Earth Planet. Sci. Lett.* **139,** 471–483 (1996).
19. Fisher, C. R. *et al.* Methane ice worms: *Hesiocaeca methanicola* colonizing fossil fuel reserves. *Naturwissenschaften* **87,** 184–187 (2000).
20. Paull, C. K., Matsumoto, R. & Wallace, P. *Proc. ODP Init. Rep.* **164** (1996).
21. Korenaga, J., Holbrook, W. S., Singh, S. C. & Minshull, T. A. Natural gas hydrates on the southeast U.S. margin: Constraints from full waveform and travel time inversions of wide angle seismic data. *J. Geophys. Res.* **102,** 15345–15365 (1997).

Acknowledgements We thank C. Voss for advice on finite element modelling.

Competing interests statement The authors declare that they have no competing financial interests.

Correspondence and requests for materials should be addressed to W.W. (e-mail: warren.wood@nrlssc.navy.mil).

Unconventional lift-generating mechanisms in free-flying butterflies

R. B. Srygley & A. L. R. Thomas

Department of Zoology, University of Oxford, South Parks Road, Oxford OX1 3PS, UK

Flying insects generate forces that are too large to be accounted for by conventional steady-state aerodynamics[1,2]. To investigate these mechanisms of force generation, we trained red admiral butterflies, *Vanessa atalanta*, to fly freely to and from artificial flowers in a wind tunnel, and used high-resolution, smoke-wire flow visualizations to obtain qualitative, high-speed digital images of the air flow around their wings. The images show that free-flying butterflies use a variety of unconventional aerodynamic mechanisms to generate force: wake capture[3], two different types of leading-edge vortex[3–7], active and inactive upstrokes[8], in addition to the use of rotational mechanisms[3] and the Weis–Fogh 'clap-and-fling' mechanism[9–12]. Free-flying butterflies often used different aerodynamic mechanisms in successive strokes. There seems to be no one 'key' to insect flight, instead insects rely on a wide array of aerodynamic mechanisms to take off, manoeuvre, maintain steady flight, and for landing.

Recent experiments with tethered hawkmoths, and with large-scale mechanical flapping models, have successfully replicated some of the force-generating abilities of insects[3–7]. Leading-edge vortices form over the wings of both hawkmoths and models during the downstroke. A vortex held above a wing has long been known to be capable of generating lift[2,13–19]. A transient leading-edge vortex can be formed by sudden changes in flow velocity[20] or pitch[21], and aerodynamic experiments in unsteady flows have shown that at its peak, the vortex can increase the lift coefficient markedly above the steady-state value for a given aerofoil[2,20,21]. Studies with model insects[3,6,7] suggest that leading-edge vortices can be quite stable over model insect wings, and may produce a twofold increase in lift. There are at least two other aerodynamic mechanisms involved in insect flight: one associated with wing rotation[1,3,7] and another associated with wake capture[3,7]; however, until now the flow features associated with wake capture and rotational mechanisms have not been identified in real insects, even in tethered flight.

There are also qualitative differences between the published structures of the leading-edge vortices formed over two flapper models[3,5–7]. The flow field around the hawkmoth flapper model is apparently analogous to the leading-edge vortices over delta wings, with vortex stability maintained by the removal of vorticity through a spanwise (base of the wing to the wing-tip) axial flow along the vortex cores[5,6]. However, chordwise fences on the wings of the *Drosophila* flapper model stopped spanwise flow but not the leading edge vortex, which even increased in size and strength[3]. Flow visualization experiments with tethered hawkmoths showed leading-edge vortices[5,6], but with insufficient resolution to reveal the internal structure. Furthermore the hawkmoths were tethered, and although an insect on a tether may flap its wings, this is not real flight.

To overcome the problems associated with tethered insects, we used a high-resolution, flow visualization system to examine the details of the field of air flow around the wings of free-flying butterflies (*Vanessa atalanta*). To describe the topology of the different three-dimensional separated flows that free-flying butterflies produce, we used critical point concepts[22–27].

The butterflies in our experiments used all of the unsteady aerodynamic mechanisms that have been proposed. They switch between mechanisms freely—often using completely different mechanisms on successive wing strokes—and are able to choose different aerodynamic mechanisms to suit different flight behaviours. Visualizations of air flow in free flight show that the fluttering of butterflies is not a random, erratic wandering, but results from the mastery of a wide array of aerodynamic mechanisms available to free-flying insects.

Figure 1a shows the typical flow field over the midline of a butterfly during a downstroke. The flow is clearly not of the type described in previous studies[3,5,7] and of that shown in Fig. 1b. Instead, an open U-shaped separation exists above the insect with a free-slip critical point (saddle) above the midline. This distinct pattern of leading-edge vortex flow has a nodal point of attachment on the midline. Lines of attachment run from this nodal-point along the undersurface of the wings to the wing-tips; there is a saddle point of separation on the top surface of the body from which lines of separation run to the wing-tips close to, or along, the leading edge. There is a free-slip critical point (saddle) above the midline, and the leading-edge vortices extend out from this free-slip critical point along the wings and on into the wing-tip vortices (with which they are continuous). The leading-edge vortices are not conical or spiral in any of our images, but are of approximately constant diameter, and if there is any spanwise flow it is too weak to be detected. In such images, spanwise flow would appear as a distortion of the curved smoke streams passing round the leading-edge vortex, with streams nearer the centre of the leading-edge vortex being pulled out towards the wing-tips or even turning to flow along the wings towards the wing-tips. This sort of distortion is not visible in any of our flow visualizations of *V. atalanta*. Re-attachment occurs either at a nodal point of attachment on the rear of the body from which lines of attachment run to the wing-tips, or at a free-slip

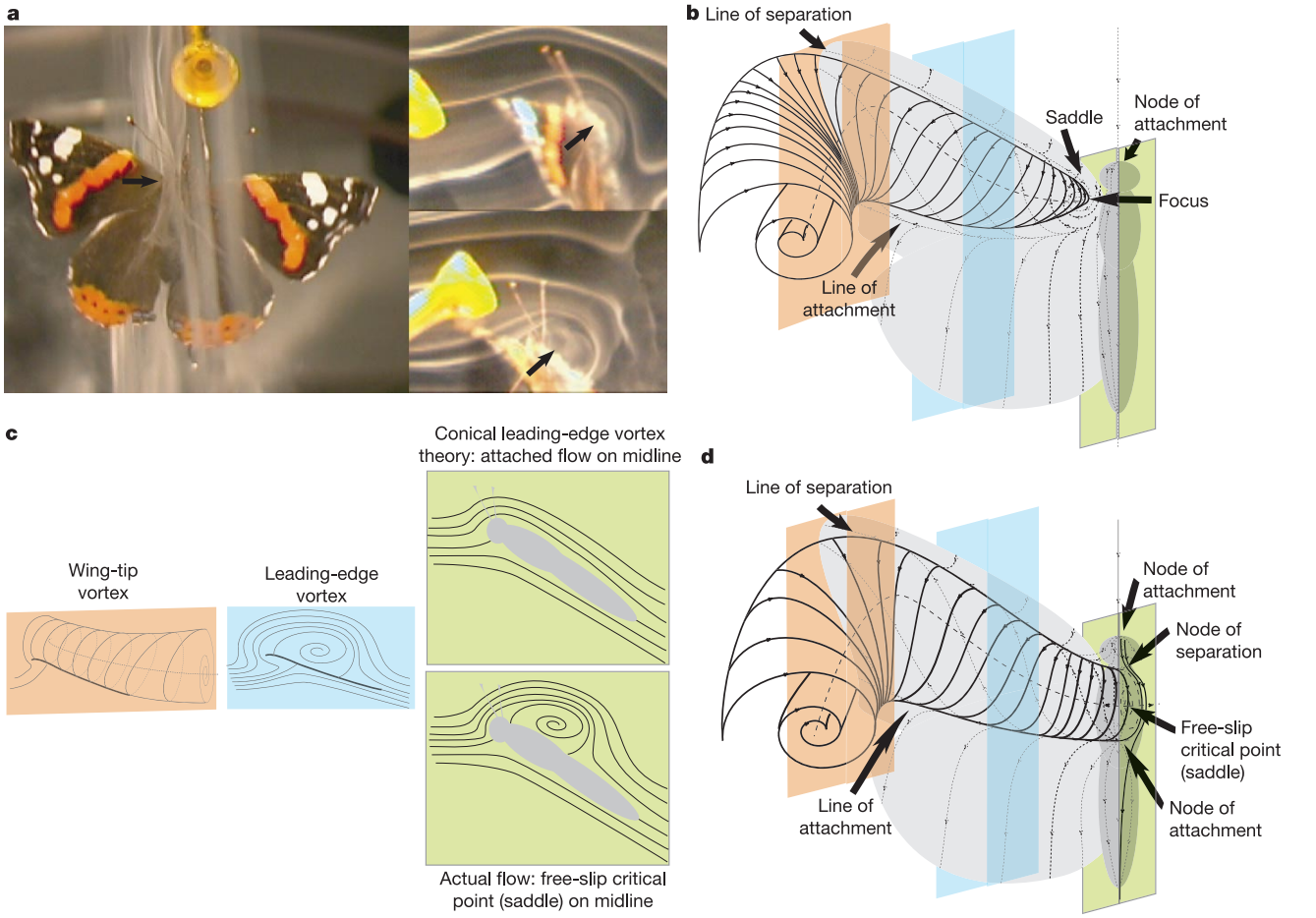

Figure 1 Butterfly leading edge vortex structure. **a**, Smoke-wire visualization of the flow over the midline of *V. atalanta* in free flight. Top and side views of a 397-mg female flying into a 1.5 m s^{-1} wind are shown. The high-speed camera images were taken immediately before and after the high-resolution top view. The images show a free-slip critical point (saddle) above the midline of the animal (arrows). **b**, Critical point reconstruction of the flow described from tethered flight and flapping flight studies[2,4,5] with conical-spiral leading-edge vortices (Werle–Legendre separations) over each wing and attached flow over the midline. The flow seen in **a** is not consistent with this pattern of flow. **c**, Side views showing the flow that would be visualized by a vertical array of smoke streams positioned along the midline, half-way out along the wing, and at the wing-tip. The conical-spiral leading-edge vortices would require an attached flow at the midline, which is not seen in *V. atalanta*. **d**, Critical point interpretation of the flow that is seen in flow visualizations of *V. atalanta*. There is a free-slip critical point (saddle) above the midline of the animal, and the cores of the leading-edge vortices run from this saddle point out along the leading edges and into the wing-tip vortices, with which they are continuous. The leading-edge vortices are of constant diameter, and spanwise flow is negligible or absent (see Supplementary Information for video footage and further images showing these details).

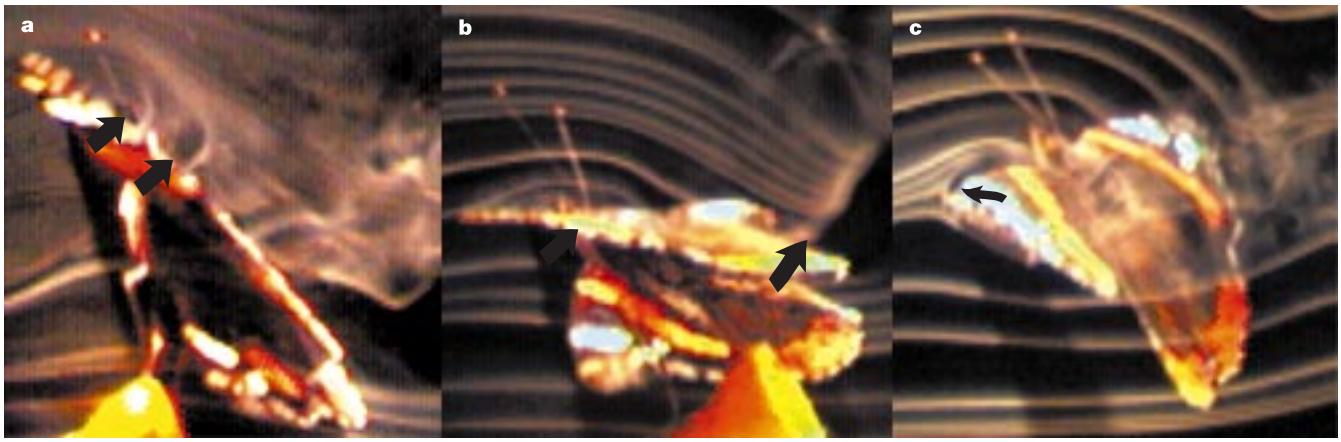

Figure 2 Flow over the wings during the downstroke. **a**, Side view of a double leading-edge vortex (arrows) used to generate extreme accelerations in vertical take off by a 364-mg male flying into a 1.0 m s^{-1} wind. **b**, Attached flow used by a 434-mg male during steady forward flight into a 1.5 m s^{-1} wind. The arrow points to the bright smoke streams flowing straight towards the camera as they wrap around the wing-tip vortex. **c**, Leading-edge vortex used during acceleration by the same 434-mg male in the same video sequence. The arrow points to a smoke stream that splits in front of and above the leading edge where it encounters the rapidly rotating air in the leading-edge vortex, which is moving vertically at this point; that is, in a perpendicular direction to the smoke stream arriving at the wing.

critical point (node) behind the body from which bifurcation lines run to the wing-tips. Again saddle points of separation will be present at the wing-tips. Figure 1d is a sketch of the main features and critical points of this type of flow field. Smoke visualization is a qualitative technique which cannot pick up subtle variations in velocity in a flow field, but the huge separation over the midline in Fig. 1a and the clear and unequivocal presence of a free-slip critical point above the midline rules out the conical-spiral leading-edge vortex theory previous work had suggested. It would not be possible for single-winged flappers to accurately reproduce the flow seen in Fig. 1a, so their results[3,5–7] should be viewed with caution.

The leading-edge vortices are present over the wings from the beginning of the downstroke. *Vanessa atalanta* uses a variant of the Weis–Fogh and Lighthill's clap-and-fling mechanism (the clap and peel) to start the downstroke (usually), and the leading-edge vortices appear fully formed as soon as the wings separate—our visualizations do not reveal any substantial change in the size or form of the leading-edge vortices during the wing-beat (as might be expected in a dynamic stall mechanism). The clap and peel, and the formation of the leading-edge vortices can be seen in the video sequences provided as Supplementary Information.

Our visualizations show *V. atalanta* using the leading-edge vortex mechanism for gentle acceleration or manoeuvres, and for climbing flight; however, our visualizations of steady forward flight or of rapid accelerations show qualitatively different flow patterns. Figure 2 shows three types of flow over the wings of the butterfly during downstrokes.

During wing-beats that result in very large accelerations of the butterfly, our visualizations show *V. atalanta* producing two sub-parallel leading-edge vortices over the top surface of the wing (Fig. 2a). High-speed video footage shows that the two vortices form during two phases of acceleration at the start of the wing-beat—the initial peel at the start of the downstroke and a subsequent acceleration once the wings have separated. They have the same sense of rotation so they are not equivalent to the primary and secondary vortices seen over delta wings[20].

In steady forward flight we find no evidence of a leading-edge vortex in *V. atalanta*. The leading-edge vortex is part of a high-lift mechanism, which may also generate large drag. Any fluid captured in the leading-edge vortex loses streamwise velocity as it is accelerated into the flow of the leading-edge vortex[8,15]. Theoretical[4,7,8,16] and experimental[7,13–15] analyses show that the lift to drag ratio is higher under attached flow conditions than when flow is separated to form a leading-edge vortex. High lift is not required for steady forward flight, so the absence of a leading-edge vortex (Fig. 2b) in forward free flight in our experimental butterflies makes sense from an energetics perspective. The existence of a large leading-edge vortex in previous work with hawkmoths and particularly its increase in size in fast forward flight[28] is puzzling, and may be an artefact of tethering. Flow visualization with free-flying hawkmoths is required.

During the final stages of the downstroke in *V. atalanta* there is often (but not always) a phase where the wing stops translating, and instead rotates in a nose-up sense. The aerodynamics of rotational mechanisms are well known for cylinders rotating in a steady flow[1,2]. Wing rotation can also produce circulation, and this rotational circulation adds to the normal translational circulation[1–3]. This is demonstrated most clearly in one of the video sequences (see Supplementary Information) at the end of the second wing-beat where the size of the wing-tip vortex increases substantially as the wings rotate rapidly at the end of the downstroke.

At the ends of the wing strokes when the wing stops, circulation is shed into the wake in the form of discrete energetic stopping vortices. A wing passing through a stopping vortex could extract energy from it if correctly orientated[3,7]. Optimally, to save energy, wake capture would increase the size of the stopping vortex (increasing the mass flow in the wake) while reducing the circulation of the stopping vortex (reducing the velocity in the wake). The same momentum (mv) could be shed into the wake at a lower cost in terms of kinetic energy ($1/2\ mv^2$). Alternatively, wake capture could involve the extraction of circulation from the stopping vortex to form the bound vortex on the wing for the next stroke, or to

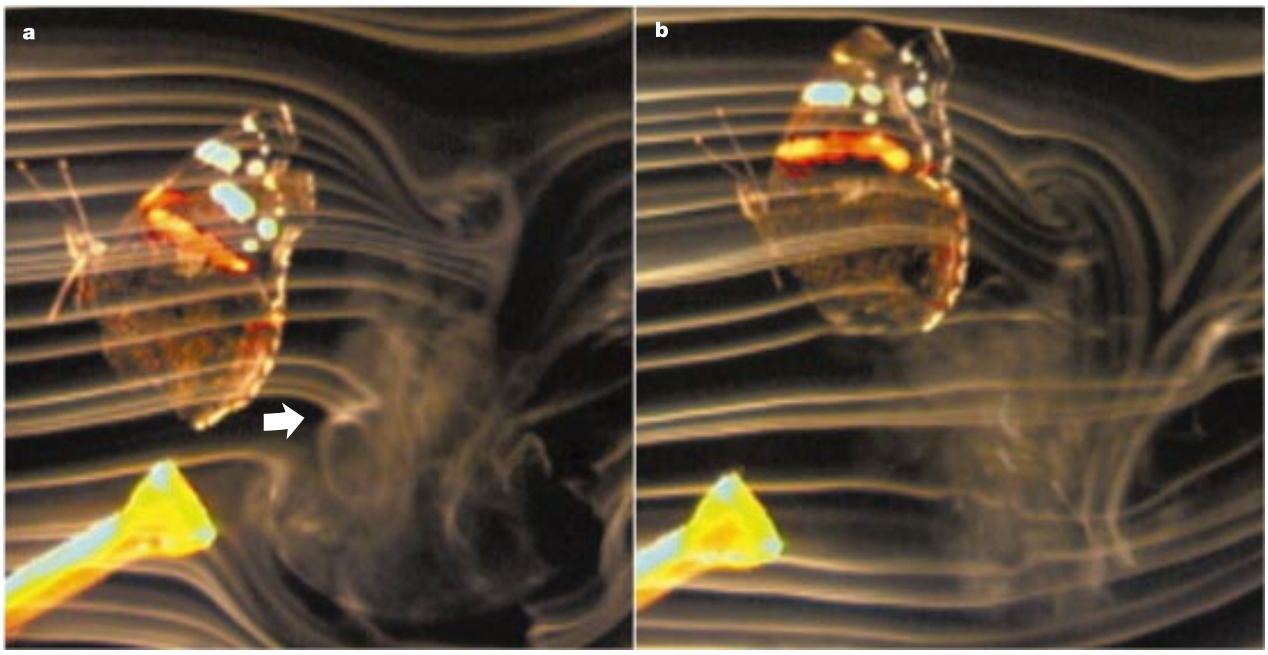

Figure 3 Wake capture. The images show successive wing-beats by a 434-mg male flying into a 1.5 m s^{-1} wind. **a**, The wing-beat has produced a wake structure with a clearly defined stopping vortex marked by the curved smoke streams at the arrow. No wake capture has occurred. **b**, Instead of a small, high-velocity stopping vortex marked by curved smoke streams behind and below the insect, there is a large area of disorganized smoke at the lower right of the image. The wing has moved through the stopping vortex on the subsequent upstroke, disrupting the structure of the stopping vortex.

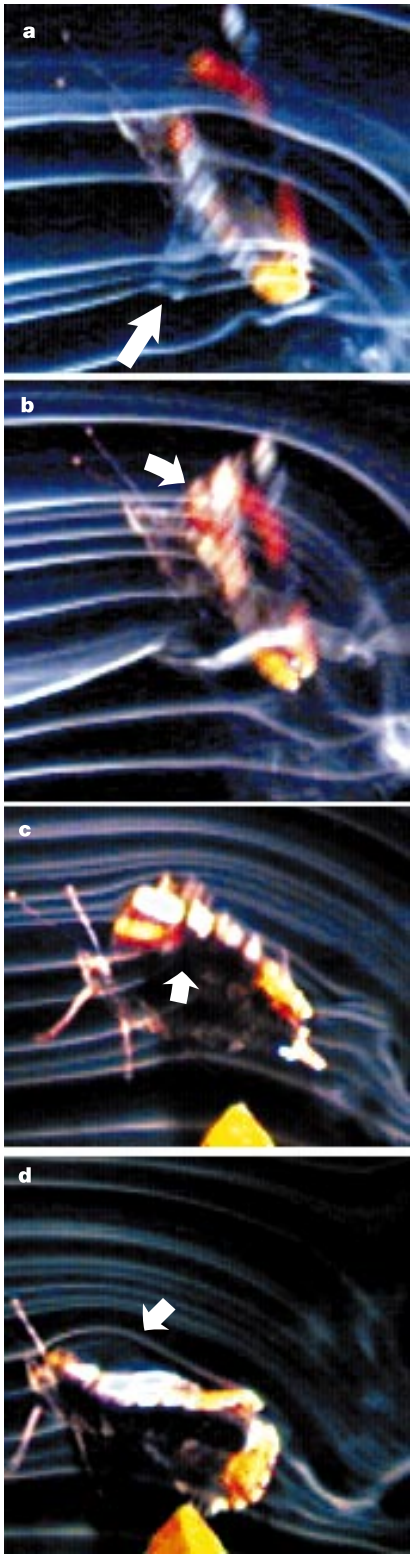

Figure 4 Upstrokes with positive, neutral and negative (downwards) loadings produced during a single flight by a 434-mg male flying into a 1.5 m s^{-1} wind. **a**, Disjointed smoke streams indicative of a downward-loaded upstroke, and the wing-tip vortex is clearly visible (arrow). The upstroke in this case would produce forwards and downwards forces. **b**, The smoke streams are undisturbed by the passage of the wing (arrow), indicating that the wing is unloaded. **c**, A positively loaded upstroke, and the curvature of the smoke streams close to the stagnation point (arrow), indicate positive circulation around the wing. **d**, Positive circulation and a leading-edge vortex (arrow) on the upstroke. This upstroke would be generating forces directed upwards and backwards.

accelerate the wing by the interaction of the near-stationary wing with the accelerated flow around it (added mass force).

Figure 3 shows the wake at the late upstroke stage in two wing-beats—one with wake capture (Fig. 3b) and one without (Fig. 3a). The effect of wake capture is clear in the difference between these frames. When the upstroke is configured so that the wing interacts with the stopping vortex, the structure of the stopping vortex is disrupted, increasing the mass of fluid in motion but decreasing the intensity of its rotation. The flow visualizations in Fig. 3 are entirely consistent with the use of wake capture as a way of increasing the efficiency of the flight mechanism by increasing the mass at the same time as reducing the velocity in the stopping vortex.

Free-flying butterflies use a wide array of different aerodynamic mechanisms in flight. In successive wing-beats, *V. atalanta* can choose to use, or not to use, wake capture, leading-edge vortices, a clap and peel mechanism, and whether to use positive, negative or zero loading on the upstroke (Fig. 4; see also Supplementary Information).

In birds and bats the loading on the upstroke changes from negative or zero at low speeds to positive at higher speeds in a manner analogous to the gait changes of terrestrial animals[29,30]. *Vanessa atalanta*, in contrast, uses radically different aerodynamic mechanisms on successive wing-beats, rather than successive gaits at different speeds.

Our results show a clear correlation between the aerodynamic mechanism that *V. atalanta* selects and the acceleration produced by that wing-beat. *Vanessa atalanta* selects leading-edge vortex mechanisms, clap and peel, and rotational mechanisms when it requires very high lift forces, and avoids them in steady forward flight.

The micro-air-vehicle community may find it daunting that the first flow visualizations of free-flying insects have revealed such a wide range of aerodynamic mechanisms, and that the insect switches between them on successive wing strokes with apparent ease. The situation may not be as complex as it first seems, because inspection of the flow visualization videos suggests that *V. atalanta* switches between different aerodynamic mechanisms through rather simple changes in wing-beat kinematics. For example, the difference between wing-beats with and without wake capture is that in wake-capture events there is less anterior motion of the wing at the end of the downstroke. Relatively subtle changes in kinematics can change radically the aerodynamic mechanism that the insect uses. The rapid shift between aerodynamic mechanisms and consequent large changes in the forces produced per wing stroke may be why butterflies flutter. □

Methods

Equipment and experimental design

Butterflies were captured at the Oxford University Zoology Department and trained to feed from an artificial feeder (golf tee). The feeder was then positioned in a low-turbulence, low-noise wind tunnel operating at a range of speeds from 0.5 to 2.5 m s^{-1}. Butterflies were filmed after feeding and shivering to warm up; hence, all video sequences used in the analyses were of natural, self-motivated free flight. Smoke streams were generated by the smoke-wire technique (Horners steam engine oil on electrically heated 0.1-mm nichrome wire). An array of direct current spotlights giving a total of 650 W provided even overhead illumination. Butterflies were filmed using two Canon XL1 camcorders, four Canon MV30DV camcorders and high-speed video (NAC500, 250 frames per second). Multiple cameras were used to provide stereo and orthogonal views to permit reconstruction of the highly three-dimensional, unsteady flows produced by the insects. Images presented here are from Vanessa11, Vanessa5 and Vanessa4 sequences. Quicktime versions of the original video and a set of supplementary figures are available as Supplementary Information. The images presented here are taken from the original, undistorted 640 × 480 pixel digital video images. No image manipulation has been performed other than the addition of arrows or labels to the figures.

Critical point theory

In unsteady separated flows, streamlines converge on or diverge from particular points, and the streamline vector is undefined at those singular critical points[24–27]. For example, where the flow attaches at the front of a sphere there is a single attachment point and streamlines on the surface radiate out from this critical point, which is called a node[23,27]. The direction of the flow at the nodal point of attachment is undefined. The other

common types of critical point are foci[23,27] (such as the point on the surface where the centre of a vortex touches down) and saddles[23,27] (which have two streamlines entering and two leaving the critical point from opposite directions). Saddle points are thought to be characteristic of separated flows[21–24]. The distribution of critical points, and of the streamlines joining them, defines the topology of the flow, and obeys topological rules[23,24]. For example, the number of nodes plus foci must equal the number of saddles plus 2 in the skin friction lines on a body surface, just as faces plus corners equals edges plus 2 for a solid body such as a cube.

Received 26 March; accepted 7 October 2002; doi:10.1038/nature01223.

1. Sane, S. P. & Dickinson, M. H. The aerodynamic effects of wing rotation and a revised quasi-steady model of flapping flight. *J. Exp. Biol.* **205,** 1087–1096 (2002).
2. Zbikowski, R. On aerodynamic modelling of an insect-like flapping wing in hover for micro air vehicles. *Phil. Trans. R. Soc. Lond. A* **360,** 273–290 (2002).
3. Dickinson, M. H., Lehmann, F.-O. & Sane, S. P. Wing rotation and the aerodynamic basis of insect flight. *Science* **284,** 1954–1960 (1999).
4. Maxworthy, T. The fluid-dynamics of insect flight. *Ann. Rev. Fluid Mech.* **13,** 329–350 (1981).
5. Ellington, C. P., van den Berg, C., Willmott, A. P. & Thomas, A. L. R. Leading-edge vortices in insect flight. *Nature* **384,** 626–630 (1996).
6. Van den Berg, C. & Ellington, C. P. The vortex wake of a hovering model hawkmoth. *Phil. Trans. R. Soc. Lond B* **352,** 317–328 (1997).
7. Birch, J. M. & Dickinson, M. H. Spanwise flow and the attachment of the leading-edge vortex on insect wings. *Nature* **412,** 729–733 (2001).
8. Saffman, P. G. & Sheffield, J. S. Flow over a wing with an attached free vortex. *Studies Appl. Math.* **57,** 107–117 (1977).
9. Weis-Fogh, T. Quick estimates of flight fitness in hovering animals, including novel mechanisms for lift production. *J. Exp. Biol.* **59,** 169–230 (1973).
10. Lighthill, J. On the Weis-Fogh mechanism of lift generation. *J. Fluid Mech.* **60,** 1–17 (1973).
11. Maxworthy, T. Experiments on the Weis-Fogh mechanism of lift generation by insects in hovering flight. Part 1. Dynamics of the 'fling'. *J. Fluid Mech.* **93,** 47–63 (1979).
12. Ellington, C. P. *Biological Fluid Dynamics* Symp. Soc. Exp. Biol. (eds Ellington, C. P. & Pedley, T. J.) Vol. 49, 109–129 (Company of Biologists, Cambridge, 1995).
13. Rossow, V. J. Lift enhancement by an externally trapped vortex. *J. Aircraft* **15,** 618–625 (1978).
14. Rossow, V. J. Two-fence concept for efficient trapping of vortices on airfoils. *J. Aircraft* **29,** 847–855 (1992).
15. Rossow, V. J. Aerodynamics of airfoils with vortex trapped by two spanwise fences. *J. Aircraft* **31,** 146–153 (1994).
16. Huang, M.-K. & Chow, C.-Y. Trapping of a free vortex by Joukowski airfoils. *Am. Inst. Aeronaut. Astronaut. J.* **20,** 292–298 (1982).
17. Mourtos, N. J. & Brooks, M. Flow past a flat plate with a vortex/sink combination. *J. Appl. Mech.* **63,** 543–550 (1996).
18. Riddle, T. W., Wadcock, A. J., Tso, J. & Cummings, R. M. An experimental analysis of vortex trapping techniques. *J. Fluids Eng.* **121,** 555–559 (1999).
19. Gursul, I. & Ho, C.-M. High aerodynamic loads on an airfoil submerged in an unsteady stream. *Am. Inst. Aeronaut. Astronaut. J.* **30,** 1117–1119 (1992).
20. Gad-el-Hak, M. & Ho, C.-M. Unsteady vortical lift around three-dimensional lifting surfaces. *Am. Inst. Aeronaut. Astronaut. J.* **24,** 713–721 (1986).
21. Délery, J. M., Legendre, R. & Werlé, H. Toward the elucidation of three-dimensional separation. *Ann. Rev. Fluid Mech.* **33,** 129–154 (2001).
22. Perry, A. E. & Chong, M. S. A description of eddying motions and flow patterns using critical-point concepts. *Ann. Rev. Fluid Mech.* **19,** 125–155 (1987).
23. Tobak, M. & Peake, D. J. Topology of three-dimensional separated flows. *Ann. Rev. Fluid Mech.* **14,** 61–85 (1982).
24. Lighthill, M. J. *Laminar Boundary Layer Theory Section II 2.6* (ed. Rosenhead, L.) 72–82 (Oxford Univ. Press, New York, 1963).
25. Legendre, R. Separation de L'ecoulement laminaire tridimensionnel. *Rech. Aeronaut.* **54,** 3–8 (1956).
26. Poincaré, H. Les points singulièrs des équations différentielles. *C.R. Acad. Sci. Paris* **94,** 416–418 (1882).
27. Hornung, H. & Perry, A. E. Some aspects of three-dimensional separation. I: Streamsurface bifurcations. *Z. Flugwiss. Weltraumforsch.* **8,** 77–87 (1984).
28. Willmott, A. P., Ellington, C. P. & Thomas, A. L. R. Flow visualisation and unsteady aerodynamics in the flight of the hawkmoth *Manduca sexta*. *Phil. Trans. R. Soc. Lond. B* **352,** 303–316 (1997).
29. Rayner, J. M. V., Jones, G. & Thomas, A. L. R. Vortex flow visualizations reveal change in upstroke function with flight speed in bats. *Nature* **321,** 162–164 (1986).
30. Spedding, G. R. *Advances in Comparative Environmental Physiology 11. Mechanics of Animal Locomotion* (ed. Alexander, R. M.) (Springer, Berlin, 1993).

Supplementary Information accompanies the paper on *Nature*'s website (http://www.nature.com/nature).

Acknowledgements We thank the Engineering and Physical Sciences Research Council instrument pool for use of their NAC500 high-speed video camera. R.B.S. was supported by a Biotechnology and Biological Sciences Research Council grant to A.L.R.T. A.L.R.T. was supported by a Royal Society University Research Fellowship.

Competing interests statement The authors declare that they have no competing financial interests.

Correspondence and requests for materials should be addressed to A.L.R.T. (e-mail: adrian.thomas@zoo.ox.ac.uk).

Sex releases the speed limit on evolution

Nick Colegrave

Institute of Cell, Animal and Population Biology, University of Edinburgh, Edinburgh EH9 3JT, UK

Explaining the evolutionary maintenance of sex remains a key problem in evolutionary biology[1–3]. One potential benefit of sex is that it may allow a more rapid adaptive response when environmental conditions change, by increasing the efficiency with which selection can fix beneficial mutations[4–7]. Here I show that sex can increase the rate of adaptation in the facultatively sexual single-celled chlorophyte *Chlamydomonas reinhardtii*, but that the benefits of sex depend crucially on the size of the population that is adapting: sex has a marked effect in large populations but little effect in small populations. Several mechanisms have been proposed to explain the benefits of sex in a novel environment, including stochastic effects in small populations, clonal interference and epistasis between beneficial alleles. These results indicate that clonal interference is important in this system.

As pointed out by Fisher[4], for sex to increase the rate of adaptation requires that the supply of beneficial mutations be abundant. If mutations arise only rarely, each is fixed before the next arises, and populations spend most of their time waiting for new mutations. Sex has little benefit under such conditions. If beneficial mutations arise more commonly, several different mutations are spreading through the population at the same time. Under such conditions, theoretical models show that clonal interference in asexual populations might place an important speed limit on adaptation, and sex should provide a significant benefit[8]. The robustness of this prediction depends to some extent on the unknown distribution of beneficial mutations, because current models of clonal interference ignore the possibility that multiple beneficial alleles arise in the same lineage[8,9]. If only a very small number of beneficial mutations (for example, two) are possible in the new environment, then the probability of both of these arising in a single asexual individual becomes non-trivial in very large populations. However, the probability that all mutations might arise simultaneously declines steeply and rapidly with the number of possible beneficial mutations. In this situation it seems likely that the genotypes carrying different subsets of beneficial alleles interfere in the same way as for a single mutation[9]. Furthermore, there is experimental evidence that clonal interference does occur in asexual populations of bacteria and viruses[9,10].

Because large populations have a larger number of mutations per generation than small populations, we might predict that the benefits of sex are greater in large populations. However, the effect of population size also depends on whether benefits of sex are based on stochastic associations between the beneficial mutations, which

Table 1 **Effective population size for the different experimental treatments**

Bottleneck size (N_0)	Approximate number of generations between transfers (g)	N_e
10^3	15	15,000
10^4	12	120,000
10^5	8.5	850,000
5×10^5	6.5	3,250,000
10^6	5.5	5,500,000

In common with other such microbial studies, I estimate the effective population size for beneficial substitutions (N_e) from an estimate of the number of divisions that occur in each tube between transfers (g), and the original inoculum size (N_0). $N_e = N_0 g$ (ref. 15).